# Sedimentology and magnetic fabric studies of Mio–Pliocene fluvial succession in the NW Himalayan Foreland Basin

**Article** *in* Current science · January 2009

CITATIONS
3

READS
59

**6 authors**, including:

Rajiv Kumar Sinha
Griffith University
**94** PUBLICATIONS **1,077** CITATIONS
SEE PROFILE

Koushik Sen
Wadia Institute of Himalayan Geology
**22** PUBLICATIONS **163** CITATIONS
SEE PROFILE

S.J. Sangode
Savirtibai Phule Pune University
**87** PUBLICATIONS **1,076** CITATIONS
SEE PROFILE

Sumit K Ghosh
Wadia Institute of Himalayan Geology
**45** PUBLICATIONS **763** CITATIONS
SEE PROFILE

# Sedimentology and magnetic fabric studies of Mio–Pliocene fluvial succession in the NW Himalayan Foreland Basin

**Subhajit Sinha[1,2], Koushik Sen[1], S. J. Sangode[1,3,*], Rohtash Kumar[1] and Sumit K. Ghosh[1]**

[1]Wadia Institute of Himalayan Geology, Dehra Dun 248 001, India
[2]Present address: Department of Geology, DBS (PG) College, Dehra Dun 248 001, India
[3]Present address: Department of Geology, University of Pune, Pune 411 007, India

**Magnetic fabric studies based on anisotropy of magnetic susceptibility (AMS) over mudstone facies from a 1700 m thick Mio–Pliocene Siwalik fluvial sequence infer a dominant control of tectonic fabrics as against the depositional fabrics of the associated channel sandstones. This study integrated with lithofacies variations indicates the prevalence of overall prolateness with high '*T*, *q* and *L*/*F*' values after 1100 m. Superimposition of the tectonic fabrics vis-à-vis upsection increase in frequency and thickness of the conglomerates infers greater magnitude of the tectonic signatures. The low prolateness of the fabrics between 1000 and 1100 m is inferred as the syn-tectonic lag deposits and reflects some important basin dynamic changes. The AMS approach over mudstone facies thus shows a greater scope of recording and quantifying the basin tectonic impulses in the Himalayan Foreland Basin.**

**Keywords:** Anisotropy, Himalayan Foreland Basin, magnetic susceptibility, Nurpur, Siwaliks, tectonic fabrics.

THE anisotropy of magnetic susceptibility (AMS) is a useful tool to understand sedimentary and tectonic characteristics of a weakly deformed sedimentary unit. In the past one decade numerous studies have shown the applicability of AMS in evaluating tectonic setting and fabric evolution in various kinds of sedimentary rocks like shale, mudstone and sandstone[1–8]. The bulk AMS generally provides a better understanding of the rock deformation history[9]. The AMS is usually approximated by a symmetric second-rank tensor, which can be represented as an ellipsoid with three principal axes ($K_1 \geq K_2 \geq K_3$) and their spatial orientation[10]. The magnetic fabric is reflected by the preferred orientation of mineral grains and/or mineral lattice contributing to the bulk susceptibility of a given specimen. Nevertheless, before magnetic fabrics can be interpreted as a proxy for mineral fabrics, it is necessary to identify the mineralogical sources of magnetic anisotropy because in the case of low anisotropies, even a small quantity of weakly oriented but strongly ferromagnetic minerals can overshadow the fabric of paramagnetic minerals[11].

Initiation and exhumation histories for the Himalayan Foreland Basin (HFB) have been well documented right from the Palaeocene[12,13]. Most of the terrigenous sediments of the HFB lack age diagnostic fossils and volcanic rocks/ash beds to assign stratigraphic zonations. Of late, the uplift and exhumation history of the Himalayan fold–thrust belt has advanced with incoming of systematic geochronologic data[14–17]. The Neogene uplift history of the Himalayan orogen has been reviewed by a number of authors with sedimentology[18–21], petrography[22–26] and magnetostratigraphy[14,27–30].

The Siwalik Group is one of the most important fluvial successions of the HFB, and is weakly deformed. Sangode *et al.*[5,31] and Rathi *et al.*[32] provided detailed work on AMS and magnetic fabric of the Siwalik sandstones of the Nahan sector (Subathu sub-basin) and Mohand sector (Dehra Dun sub-basin) respectively. The alignment of the principal susceptibility axes ($K_1$ and $K_2$) is pronounced in response to basin tectonic/climatic events recorded in lithounits, while the minimum susceptibility axis ($K_3$) aligns preferably to the palaeoflow direction in a majority of the Siwalik channel sands[5,31,32]. They also noted that the oblate nature of the magnetic fabric tends towards prolateness manifest tectonic signatures. In the Potwar Plateau, Pakistan, AMS studies on the Siwalik show that the sedimentary character is still retained and not completely overprinted by tectonic deformation[8]. Similar trend is also observed for the magnetic fabric in the Nepal Siwalik[14]. Assuming that AMS in the Siwalik mudstones reflects a typical pattern of depositional to tectonic fabric during progressive deformation, the aim of this article is to investigate the influence of these variables to explain the temporal trend of observed magnetic fabric. Further, these superposed fabrics are linked with the orogenic uplift histories that are based primarily on the influx and nature of conglomerate clasts.

*For correspondence. (e-mail: sangode@unipune.ernet.in)

## Location and geology

The present study was carried out along Harar Khad, north of the Jawalamukhi Thrust (JT) and towards north of Nurpur anticline (the southeasterly extension of the Suruin–Mastgarh anticline, Figures 1 and 2). This part of the foreland basin records multiple tectonic episodes that occurred during Late Eocene, Middle Miocene, Pliocene and Middle Pleistocene (<0.22 Ma)[33]. In general, the Lower Siwalik is thrusted over Upper Siwalik along JT, whereas in the study area Lower Siwalik is thrusted over the Middle Siwalik. According to Raiverman[34], along Harar Khad Enseq 5, 6 and 7 are exposed, which are equivalent to the partly Lower, Middle and Upper Siwalik Sub-groups. However, based on field observations, Sinha *et al.*[33,35] informally divided the succession into three alterations: (a) sandstone–mudstones, (b) conglomerate–sandstone–mudstone and (c) thickly bedded conglomerate. Towards north, the Siwalik Group is delimited by the Main Boundary Fault (MBF) hanging wall which comprises of the Lower Tertiary rocks[12] that occur in patches in the western Himalaya and further north lie the Lesser Himalayan succession delimited by the Main Boundary Thrust (MBT)[34].

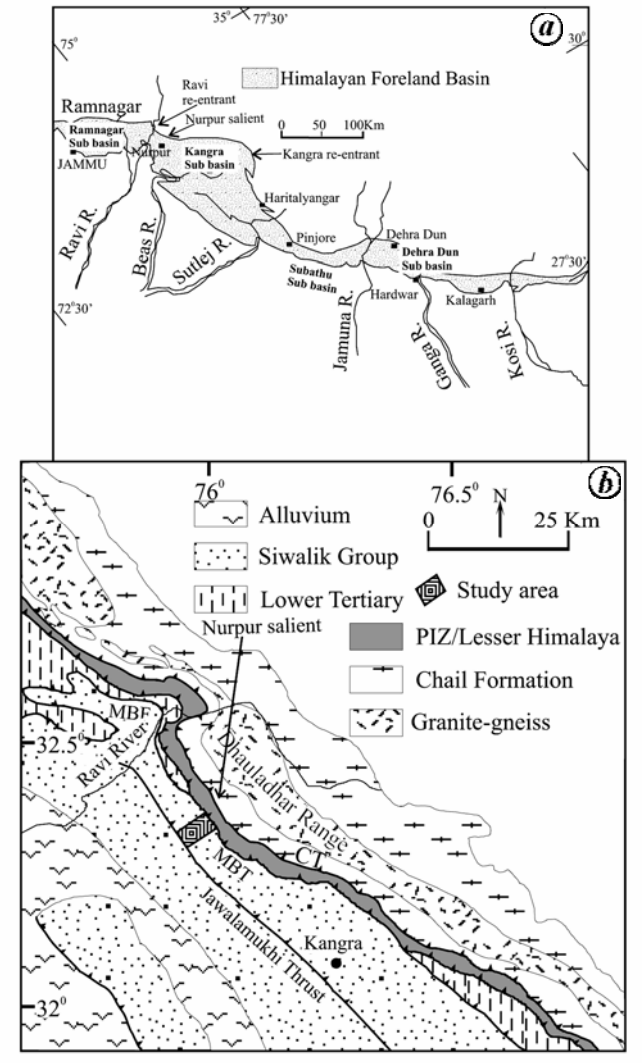


**Figure 1.** ***a***, Simplified map of Himalayan Foreland Basin (HFB) showing various sub-basins. ***b***, Geological map in and around the study area showing disposition of the various lithological units (simplified after Raiverman[34]). CT, Chail Thrust; MBT, Main Boundary Thrust; MBF, Main Boundary Fault; HFT, Himalayan Frontal Thrust; PIZ, Panjal Imbricate Zone.

## Sedimentology

The measured Harar Khad section is 1704 m thick and lies ~700 m north of JT (Figure 3). The average dip of the strata is 40° towards 70°. The three informal alternations comprise sandstone–mudstone (0–893 m), conglomerate–sandstone–mudstone (893–1518 m) and thickly bedded conglomerate (1518–1704 m, Figure 3). However, due to inaccessibility the upper part of the thickly bedded conglomerate could not be measured. The sandstone–mudstone alternation consists of both grey and buff sandstones and interbedded mudstones. The 7–16 m (occasionally reaching up to 19 m) thick, fining-upward, grey sandstones are medium- to fine-grained, laterally amalgamated, multistoried, showing sheet geometry and extend laterally for more than 500 m. Palaeoflow pattern is unimodal and shows an overall azimuthal range from 85° to 122°, with mean direction $\theta = 101°$ (Figure 3).

The buff sandstones have ribbon geometry, are fine-grained, fining upward and generally 0.8–6 m thick, encased in mudstone deposits. The base of these sand bodies is channelized and their upper contact is gradational with the overlying mudstones. The associated brownish-red mudstones have thickness varying from 1 to 38 m. The

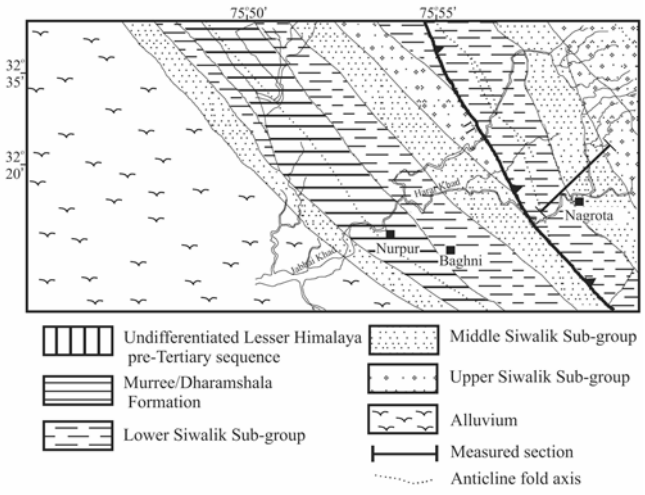


**Figure 2.** Simplified geological map of Nurpur Salient, NW part of the HFB (simplified after Raiverman[34]).

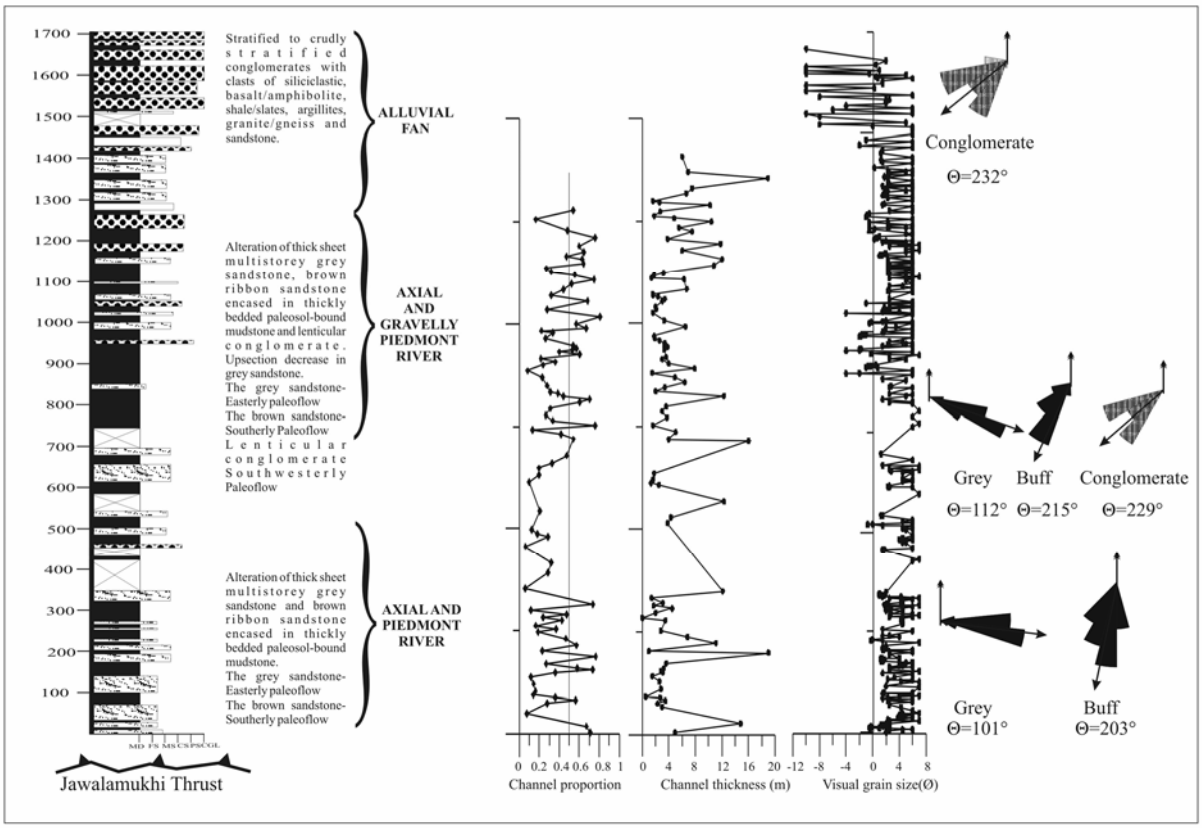


**Figure 3.** Composite diagram showing temporal variability in lithology, channel-body proportion, grain size and palaeoflow direction.

percentage of mudstone deposits in this part of the interval varies from 24 to 94 in individual cycles with an average of 68. Mudstones are generally massive and variegated, but at places parallel laminated. The mudstone horizons also contain isolated and compound mature to immature palaeosol profiles. The mature palaeosols contain abundant carbonate nodules and at places ferruginous concretions, and the immature palaeosols are without carbonate groundmass, but pedons up to 5 cm diameter are common. Soft sediment deformation features are apparent in both the grey and buff sandstones, mainly showing convolutes and load structures. The variability of palaeocurrent directions is within 175–237°, with a mean direction of 203° and with unimodal current pattern (Figure 3).

The second alternation lies between 893 and 1518 m stratigraphic interval and shows similar characteristics as present in the lower alterations, except incorporation of conglomerate with a decreasing trend in degree of pedogenesis and bioturbation. The dip of the strata is 40° towards 80° throughout this interval. The thick conglomerate bodies (0.5–2 m thick) show sheet-to-lenticular geometry and channelized base. Gradual up-section increase in average clast size proportion and frequency of conglomerate is observed (Figure 3). Overall the mean palaeocurrent direction with unimodal pattern for the buff sandstone bodies is 215° and the lensoid conglomerate is 229° (Figure 3).

Above 1518 m stratigraphic level, thickly bedded, laterally amalgamated and multistoried conglomerates are exposed and continue till the top of the measured succession. The dip of the strata is 30° towards 70° throughout this interval. The conglomerates are stratified to massive with few intercalations of medium- to coarse-grained sand lenses (<80 cm thick). Clasts are rounded and concentration of prolate clast is more compared to the oblate ones (Figure 4). The conglomerates are concentrated all along the basin margin and show rapid facies change from conglomerate-dominated to sandstone–mudstone-dominated succession. Azimuthal data obtained through clast imbrication have mean angular deviation ranging from 215° to 253°, with a grand mean of 232°, and show unimodal distribution.

## *Depositional environment*

The three alterations represent distinct fluvial systems. The first two alternations show deposits of two overlapping, SE-flowing trunk drainage and southerly flowing piedmont drainage. The third alternation is deposited in alluvial fan setting[35]. Changes in facies and their relative frequency are coeval with changes in depositional environment. Sinha *et al.*[35] inferred this as a manifestation of the episodic tectonic variability and concluded that the

shifting of the facies belts towards or away from the basin margin is in response to alternative basin subsidence and isostatic rebounding. With continued uplift of the fold-thrust belt during third alternation, sediment flux increased and conglomerate was deposited along the highly subsiding basin margin[35].

## Magnetic studies

For magnetic fabric studies, oriented non-pedogenic mudstones were collected throughout the section from fresh surfaces, taking proper precautions to avoid any contamination. The block samples (both hard and friable) were then removed from the outcrop. The hard rocks were drilled to get cores of 2.5 cm diameter and 2.2 cm length, whereas the friable samples were cut through hacksaw to obtain cubic samples. The samples were finally finished on sandpaper, washed, and later coated with fevicol for dust-free handling during laboratory procedures.

AMS was measured with KLY-3 Kappabridge (Agico, Czech Republic) in the Magnetics Laboratory, Wadia Institute of Himalayan Geology (Dehra Dun, India). Table 1 gives the orientation and magnitude of the three principal axes of the magnetic susceptibility ellipsoid ($K_1 \geq K_2 \geq K_3$). The different parameters of AMS are combinations of the corresponding eigenvalues of these three principal susceptibility axes[9,36]. The shape of the susceptibility ellipsoid is characterized by the shape parameter $T$ ($-1 \geq T \geq 1$). When $T < 0$, the ellipsoid is rod-shaped (prolate), when $T > 0$, the ellipsoid is disc-shaped (oblate). The eccentricity of the ellipsoid is measured by $P'$ ($1 \geq P' \geq$ infinity), which is related to its degree of sphericity. The parameter showing the mean susceptibility is $K_m$ (= $[K_1 + K_2 + K_3]/3$). The other important parameters are: magnetic lineation $L = K_1/K_2$, magnetic foliation $F = K_2/K_3$, and shape factor $q = (K_1 - K_2)/[(K_1 + K_2)/2 - K_3]$.

The ellipsoid shape is characterized by the parameter $T = [2(\eta_2 - \eta_3)/(\eta_1 - \eta_3)] - 1$, with $\eta_i = \ln K_i$.

**Figure 4.** Field photograph of conglomerate horizon showing high proportion of prolate clast.

## Results

### *Magnetic susceptibility*

The mean magnetic susceptibility is generally low to moderate, with values ranging from $49.2 \times 10^{-6}$ to $241 \times$

**Table 1.** Database containing different parameters of magnetic fabrics of Nurpur section

| Height (m) | $T$ | $Q$ | $P'$ | $K_m$ | $L$ | $F$ |
|---|---|---|---|---|---|---|
| 6.00 | 0.088 | 0.595 | 1.017 | 9.94E-05 | 1.008 | 1.009 |
| 30.00 | –0.241 | 0.903 | 1.012 | 1.24E-04 | 1.007 | 1.004 |
| 45.00 | –0.089 | 0.755 | 1.029 | 2.19E-04 | 1.015 | 1.013 |
| 71.00 | 0.184 | 0.515 | 1.013 | 1.10E-04 | 1.005 | 1.008 |
| 91.00 | –0.283 | 0.947 | 1.011 | 1.58E-04 | 1.007 | 1.004 |
| 114.00 | 0.267 | 0.452 | 1.018 | 7.54E-05 | 1.007 | 1.011 |
| 123.00 | 0.124 | 0.566 | 1.025 | 1.82E-04 | 1.011 | 1.014 |
| 154.00 | 0.269 | 0.45 | 1.025 | 9.33E-05 | 1.009 | 1.016 |
| 173.00 | 0.36 | 0.393 | 1.081 | 1.12E-03 | 1.025 | 1.053 |
| 216.00 | 0.599 | 0.224 | 1.02 | 1.13E-04 | 1.004 | 1.015 |
| 256.00 | 0.263 | 0.457 | 1.035 | 2.32E-04 | 1.013 | 1.022 |
| 268.00 | 0.291 | 0.433 | 1.015 | 1.73E-04 | 1.005 | 1.01 |
| 285.00 | 0.11 | 0.576 | 1.018 | 2.11E-04 | 1.008 | 1.01 |
| 295.00 | 0.376 | 0.374 | 1.032 | 1.92E-04 | 1.01 | 1.021 |
| 305.00 | –0.206 | 0.867 | 1.015 | 6.99E-05 | 1.009 | 1.006 |
| 316.00 | 0.279 | 0.444 | 1.024 | 1.66E-04 | 1.008 | 1.015 |
| 325.00 | 0.392 | 0.362 | 1.026 | 1.65E-04 | 1.008 | 1.018 |
| 335.00 | –0.185 | 0.845 | 1.014 | 9.84E-05 | 1.008 | 1.006 |
| 473.00 | –0.451 | 1.143 | 1.015 | 2.15E-04 | 1.011 | 1.004 |
| 481.00 | 0.454 | 0.32 | 1.029 | 1.72E-04 | 1.008 | 1.02 |
| 492.00 | 0.333 | 0.404 | 1.022 | 1.86E-04 | 1.007 | 1.014 |
| 508.00 | –0.001 | 0.67 | 1.011 | 1.70E-04 | 1.006 | 1.006 |
| 525.00 | 0.174 | 0.524 | 1.017 | 1.27E-04 | 1.007 | 1.01 |
| 612.00 | –0.411 | 1.094 | 1.02 | 1.94E-04 | 1.014 | 1.006 |
| 627.00 | 0.347 | 0.393 | 1.019 | 1.59E-04 | 1.006 | 1.013 |
| 652.00 | 0.354 | 0.406 | 1.141 | 1.28E-03 | 1.043 | 1.092 |
| 667.00 | 0.468 | 0.308 | 1.013 | 1.03E-04 | 1.003 | 1.009 |
| 683.00 | –0.761 | 1.575 | 1.009 | 1.48E-04 | 1.007 | 1.001 |
| 694.00 | 0.078 | 0.602 | 1.013 | 9.11E-05 | 1.006 | 1.007 |
| 822.00 | –0.368 | 1.043 | 1.013 | 8.07E-05 | 1.009 | 1.004 |
| 841.00 | 0.42 | 0.344 | 1.038 | 6.65E-05 | 1.01 | 1.026 |
| 862.00 | 0.194 | 0.509 | 1.023 | 1.24E-04 | 1.009 | 1.014 |
| 875.00 | –0.622 | 1.368 | 1.017 | 5.46E-05 | 1.013 | 1.003 |
| 903.00 | –0.528 | 1.251 | 1.068 | 7.13E-05 | 1.05 | 1.015 |
| 908.00 | 0.262 | 0.454 | 1.009 | 8.96E-05 | 1.003 | 1.005 |
| 954.00 | –0.706 | 1.488 | 1.006 | 1.29E-04 | 1.005 | 1.001 |
| 993.00 | 0.335 | 0.403 | 1.026 | 8.60E-05 | 1.008 | 1.017 |
| 1028.00 | 0.359 | 0.383 | 1.005 | 8.42E-05 | 1.002 | 1.003 |
| 1053.00 | 0.224 | 0.483 | 1.012 | 1.03E-04 | 1.005 | 1.007 |
| 1077.00 | –0.122 | 0.789 | 1.04 | 6.83E-05 | 1.022 | 1.017 |
| 1112.00 | –0.194 | 0.854 | 1.016 | 1.02E-04 | 1.009 | 1.006 |
| 1132.00 | –0.461 | 1.157 | 1.03 | 9.09E-05 | 1.021 | 1.008 |
| 1151.00 | 0.201 | 0.516 | 1.094 | 7.36E-05 | 1.036 | 1.055 |
| 1164.00 | –0.258 | 0.927 | 1.035 | 7.30E-05 | 1.022 | 1.013 |
| 1180.00 | –0.775 | 1.603 | 1.054 | 1.03E-04 | 1.043 | 1.005 |
| 1197.00 | 0.328 | 0.407 | 1.022 | 1.02E-04 | 1.007 | 1.015 |
| 1236.00 | 0.056 | 0.621 | 1.013 | 4.92E-05 | 1.006 | 1.007 |
| 1254.00 | –0.722 | 1.512 | 1.007 | 8.51E-05 | 1.005 | 1.001 |
| 1291.00 | –0.379 | 1.053 | 1.004 | 2.41E-04 | 1.003 | 1.001 |
| 1308.00 | –0.791 | 1.623 | 1.015 | 6.43E-05 | 1.012 | 1.001 |
| 1355.00 | –0.017 | 0.683 | 1.003 | 1.75E-04 | 1.002 | 1.002 |
| 1374.00 | 0.109 | 0.575 | 1.009 | 5.08E-05 | 1.004 | 1.005 |
| 1393.00 | –0.891 | 1.794 | 1.012 | 9.91E-05 | 1.01 | 1.001 |
| 1512.00 | 0.605 | 0.221 | 1.016 | 1.56E-04 | 1.003 | 1.012 |

$10^{-6}$ SI units, indicating dominance of paramagnetic and diamagnetic minerals over ferrimagnetic minerals. Only two samples, at heights of 173 and 652 m respectively, show a magnetic susceptibility $>1000 \times 10^{-6}$ SI units, indicating predominance of magnetite (Figure 5).

### *Degree of magnetic anisotropy*

The degree of anisotropy is weak with all but one sample having values >1.1. The sample showing maximum value of 1.41 is from 652 m. Since this sample also has a high susceptibility ($>1000 \times 10^{-6}$ SI units), its relatively higher degree of anisotropy can be attributed to the presence of magnetite instead of deformation (Figure 5). For samples having high mean magnetic susceptibility ($K_m > 500 \times 10^{-6}$ SI units), i.e. high concentration of magnetite, the degree of magnetic anisotropy ($P'$) cannot be correlated with strain unless $P'$ and $K_m$ are not proportional. In the present case, only samples having high $K_m$ show a relatively high value of $P'$.

### *Shape parameter*

Generally, magnetic properties of sedimentary rocks are characterized by strongly oblate fabric with shape parameter $T > 0.1$. In the present study, while 31 out of the 60 samples show $T$ value >0.1, the other 23 samples show strongly prolate fabric, i.e. $T < -0.1$. This strongly prolate nature of fabric is mostly concentrated between 800 and 1000 m stratigraphic interval and from 1100 m up-section (Figure 6).

### *Ellipsoid shape factor*

Like $T$, shape factor $q$ is also an indicator of either depositional or tectonic fabric. The $q$ value ranging from 0.06 to 0.7 is indicative of an undeformed sedimentary fabric. However, in the present study, 24 samples show a $q$ value greater than 0.7, and samples with higher value are concentrated in the upper part of the succession (Figure 6).

### *Flinn plot*

The presence of secondary fabric can also be seen in the $F$ (magnetic foliation) vs $L$ (magnetic lineation) or the Flinn diagram (Figure 7). In the Flinn plot, there is almost equal distribution of samples in the prolate and the oblate fields. As stated earlier, the oblate fabric along with low $q$ value indicates primary sedimentary fabric and samples in the prolate field indicate the presence of a secondary fabric. Figure 7 shows that the samples plot in the prolate field if $L/F$ is >1 and for oblate samples, $L/F < 1$. In the upper part above 1100 m, the sample has a strongly prolate fabric.

## Discussion

Throughout the HFB, the transition from Lower to Middle Siwalik occurred at around 10 Ma, where the fluvial architecture shows transition from minor to major sandstone

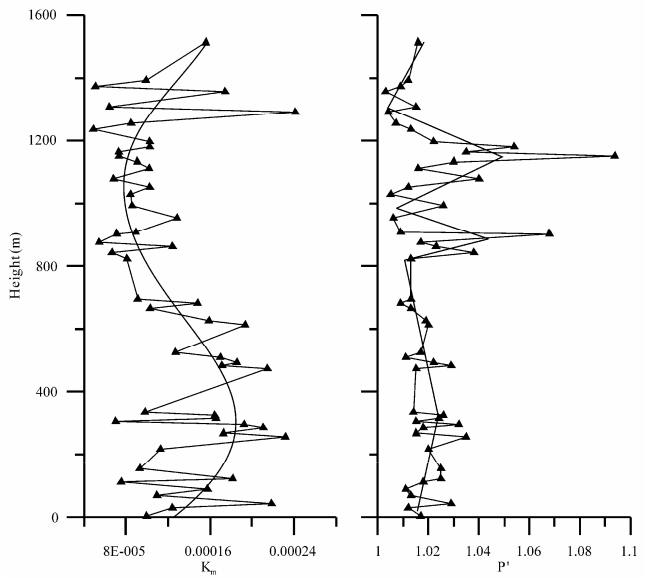


**Figure 5.** Temporal variation in $K_m$ and $P'$. Note the high $K_m$ values at 173 and 652 m stratigraphic interval, indicating the presence of magnetite. Overall $K_m$ shows no drastic variation temporally with increase in grain size at higher stratigraphic levels (see Figure 3). Removing the two peaks at 173 and 652 m, a clearer trend is observed.

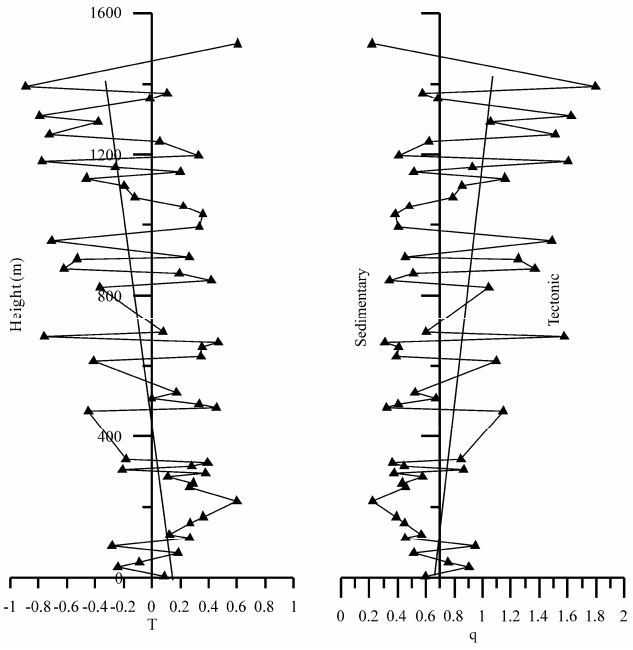


**Figure 6.** The shape parameter $T$ showing strongly prolate fabric that is mostly concentrated in the upper part in 800–1000 m interval and 1100 m onwards. This is also reflected in the shape factor $q$, where the values increase >0.7 towards the younger stratigraphic levels.

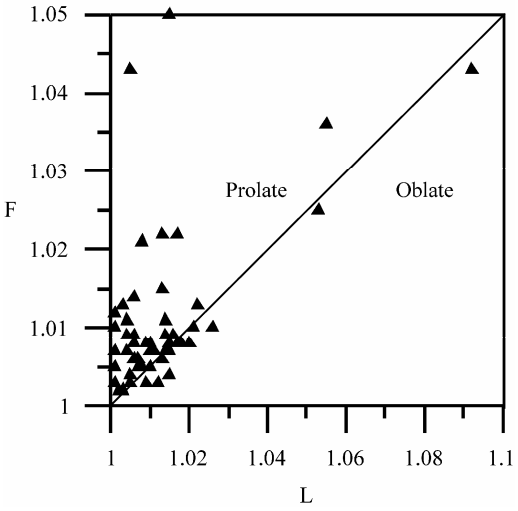


**Figure 7.** The *L*/*F* plot shows that majority of the samples fall in the prolate field, which is also comparable to the clast shape as shown in Figure 4.

bodies. The multistoried nature with abundant erosional surfaces, rare lateral accretionary surfaces and low palaeoflow variability suggest increased channel dimension with high discharge[21]. This changeover occurred at about ~11 Ma in the Potwar Plateau[27], ~10 Ma in the Kangra sub-basin[21] and ~9 Ma in Nepal[37]. Further mineralogical evidence indicates that the central crystalline zone was uplifted in response to reactivation of the Main Central Thrust (MCT) at around 10 Ma, which resulted in high relief and increased supply of metamorphic detritus[24,38,39].

In the Kangra and Ravi re-entrant, the conglomerates were deposited during Middle Siwalik (between 10 and 7 Ma), consisting of abundant metasedimentary–sedimentary fragments, granite/granite gneiss and basic clasts. This population of clasts has dominant input from Chail lithology that forms the hanging wall of the present-day Chail Thrust (CT). The clast composition of conglomerates also suggests that MCT (≈CT in the study area) was active prior to 10 Ma[22,25,39]. Interestingly, dates of thrust activities show 2–3 times acceleration in the sedimentation rate due to onset of uplift throughout the HFB from Pakistan, India and Nepal Siwalik[27–30,40].

Two sections on either side of the study area (Kangra sub-basin) have been dated through reversal magnetostratigraphy by Sangode *et al.*[30] and Sinha *et al.*[33], in the eastern and western parts respectively. These studies reveal the occurrence of Middle Siwalik conglomerate between 8.69 and 8.25 Ma in the western part, and between 9.58 and 7.37 Ma in the eastern part. The drop in the rate of sedimentation around 8.25 Ma in the eastern part[29] corresponds to the noticeable decrease in occurrence of conglomerates.

The appearance of conglomerate-rich part is accompanied by relatively high sedimentation rate in the western part of the Kangra sub-basin[30], from the period 8.69–8.25 Ma. This infers acceleration of sedimentation rate as a result of major uplift in the hinterlands prior to ~8.69 Ma. However, gravel accumulation over the underthrusting basement after 8.25 Ma suggests progradation during the quiescence period. Thus during progressive deformation and shortening of the foreland, the sediments were accommodated into the depocentre near the fold-and-thrust belt as it propagated southwards. This also indicates that as the thrust sheet advanced, the depocentre migrated towards the basin margin with change in river gradient and grain size. In the study area, three prominent alterations at 0–893, 893–1518 and 1515–1704 m stratigraphic intervals are marked by gradual influx of coarse sediments with intervening fines reflecting pulses of hinterland deformation and quiescence. Thus depositional systems in the foreland basin migrated towards or away from the basin margin in response to changes in tectonic uplift patterns. The Siwalik sediments are apparently undeformed through field observations. However, the AMS studies on the Siwalik mudstones reveal the weakly deformed nature allowing a distinction between depositional and tectonic fabrics.

AMS studies in mudstones have shown that the magnetic fabrics can undergo a series of changes during weak deformation in which distinct changes can occur in magnetic fabric ellipsoids, grading from the oblate field (sedimentary fabric) towards the prolate field (tectonic fabric)[41]. Pares[7] defined a general *Pj*–*T* (*Pj* – degree of anisotropy) path to show the development of AMS ellipsoids as the intensity of deformation increases in weakly deformed rocks and inferred height dependence of AMS fabrics as a signature of a nascent but magnetically detectable tectonic strain. Variations in sediment characteristics and the AMS parameters document the changes in transport regime and the magnitude of transportation that manifests tectonic and/or climate changes. In the Qaidam basin, Gilder *et al.*[42] showed that near the Altyn Tagh fault, the *T* parameter changed abruptly at 21 Ma from spherical on average ($T = 0$) to distinctly oblate ($T > 0$). They interpreted this as a result of change in transport conditions of the sediments. Gilder *et al.*[42] further inferred that when *T* is near 0, the particles were transported far and were sufficiently eroded to achieve a spherical shape, and the grains that travelled less distance were eroded less and were oblate on average.

In the present study gradual up-section development of prolate fabrics has been observed. The AMS fabric is thus indicative of tectonic strain due to thrust reactivation, as the rocks are subjected to N–S-directed compression since the onset of the India–Asia collision and significant crustal shortening and lithosphere thickening in this vast region of HFB. Contrary to Gilder *et al.*[42], observations of up-section oblateness of the conglomerates on average due to short distance of transport from the source are ruled out because of recycled nature of sediments in the HFB[39]. Moreover, field observations of the conglo-

merates show more prolate clasts compared to oblate ones (Figure 3). This is in contrast to the earlier studies in the adjoining eastern part of the Kangra sub-basin, where the conglomerates have prograded for several hundred kilometres[20,22,34] and are confined along the basin margin in the western part. This indicates a high basinal subsidence in the western part in comparison to the eastern region of the sub-basin. Additionally, a gradual up-section change of the tectonic fabric indicates that the conglomerates are of syntectonic origin, which is further supported by rapid facies transition from sandstone–mudstone to conglomerate-dominated succession. A decrease in the superposed fabric (low prolateness) between 1000 and 1100 m is due to syn-tectonic lag of the sediments immediately after tectonic activity.

The rapid uplift of the Tibetan Plateau and Himalaya appears[43] to have been initiated prior to 13.7 Ma. Since then, there has been onset of the monsoon with intermittent dry and intense wet phases[44,45]. While it is acknowledged that regionally there were monsoonal dry and intense phases, the local climatic changes also contributed to the increase in erosion and accumulation rates. These local changes in the tectono-climatic regime are due to the formation of different tectonogenic blocks controlled by subsurface topography, basement rigidity and hinterland tectonic framework separated by transverse lineaments causing differential activity of thrust belts throughout the foreland[25,46]. In the present study area, it is apparent from the temporal magnetic susceptibility plots that magnetic mineralogy had remained almost uniform throughout the depositional milieu (Figure 4). Sinha *et al.*[48] have also shown relatively uniform geochemical signatures along the adjacent western region. Thus it seems that climate remained almost similar throughout the basin-fill stratigraphy. Therefore, increase in $T$, $q$ and $L/F$ parameters and gradual up-section increase of conglomeratic interlayers and conglomerate bed thickness reflect mountain uplift in response to thrust activity.

## Conclusion

The sedimentologic and AMS study of the Neogene succession along Nurpur Salient gives the following inferences:

1. The AMS of mudstone forms a reliable tool to differentiate between the primary depositional and the superposed tectonic fabrics and can reflect the variability in subsidence history and changes in the fabric parameters ($K_m$, $P'$, $T$) useful as a proxy to the change in tectonic regime.
2. The magnetic fabric studies in agreement with the syntectonic, coarse-grained facies in the study area clearly reflect the dominating control of tectonic fabrics, reflecting the changes in basin accommodation space and relief. It also suggests that although climate is equally significant, the tectonic readjustments give the final imprints to the basin-sediment architecture.


1. Averbuch, O., Frizon de Lamotte, D. and Kissel, C., Magnetic fabric as a structural indicator of the deformation path within a fold–thrust structure: a test case from the Corbieres (NE Pyrenees, France). *J. Struct. Geol*., 1992, **14**, 461–474.
2. Sagnotti, L. and Speranza, S., Magnetic fabrics analysis of the Plio–Pleistocene clayey units of the Sant'Arcangelo basin, Southern Italy. *Phys. Earth Planet. Inter*., 1993, **77**, 165–176.
3. Mattei, M., Sagnotti, L., Faccenna, C. and Funiciello, R., Magnetic fabric of weakly deformed clay-rich sediments in the Italian peninsula: Relationships with compressional and extensional tectonics. *Tectonophysics*, 1997, **271**, 107–122.
4. Liu, B., Saito, Y., Yamazaki, T., Abdeldayem, A., Oda, H., Hori, K. and Zhao, Q., Paleocurrent analysis for the late Pleistocene–Holocene incised-valley fill of Yangtze delta, China by using anisotropy of magnetic susceptibility data. *Mar. Geol.*, 2001, **176**, 175–189.
5. Sangode, S. J., Kumar, R. and Ghosh, S. K., Application of magnetic fabric studies in an ancient fluvial sequence of NW Himalaya. *Curr. Sci.*, 2001, **81**, 66–71.
6. Parés, J. M., van der Pluijm, B. and Dinarès-Turell, J., Evolution of magnetic fabrics during incipient deformation of mudrocks. *Tectonophysics*, 1999, **307**, 1–14.
7. Pares, J. M., How deformed are weakly deformed mudrocks? Insights from magnetic anisotropy. In *Magnetic Fabric: Methods and Applications* (eds Martin-Fernandez, F. *et al.*), Geological Society of London, 2004, vol. 238, pp. 191–203.
8. Robion, P., Grelaud, S. and Lamotte, D. F., Pre-folding magnetic fabrics in fold-and-thrust belts: Why the apparent internal deformation of the sedimentary rocks from the Minervois basin (NE-Pyrenees, France) is so high compared to the Potwar basin (SW-Himalaya, Pakistan)? *Sediment. Geol.*, 1007, **196**, 181–200.
9. Tarling, D. H. and Hrouda, F., *The Magnetic Anisotropy of Rocks*. Chapman and Hall, London, 1993, p. 217.
10. Borradaile, G. J. and Tarling, D. H., The influence of deformation mechanisms on magnetic fabrics in weakly deformed rocks. *Tectonophysics*, 1981, **77**, 151–168.
11. Borradaile, G. J. and Werner, T., Magnetic anisotropy of some phyllosilicates. *Tectonophysics*, 1994, **235**, 223–248.
12. Singh, B. P., Evidence of growth fault and forebulge in the Late Paleocene (57.9–54.7 Ma), western Himalayan foreland basin, India. *Earth Planet. Sci. Lett*., 2003, **216**, 717–724.
13. DeCelles, P. G., Robinson, D. M., Quade, J., Ojha, T. P., Garzione, C. N., Copeland, P. and Upreti, B. N., Stratigraphy, structure, and tectonic evolution of the Himalayan fold-thrust belt in western Nepal. *Tectonics*, 2001, **20**, 487–509.
14. Gautam, P. and Rosler, W., Depositional chronology and fabric of Siwalik Group sediments in central Nepal from magnetostratigraphy and magnetic anisotropy. In *Geology of the Nepal Himalaya, Recent Advances* (eds LeFort, P. and Upreti, B. N.), *J. Asian Earth Sci.*, 1999, **17**, 659–682.
15. Wobus, C., Heimsath, A., Whipple, K. and Hodges, K., Active out-of-sequence thrust faulting in the central Nepalese Himalaya. *Nature*, 2005, **434**, 1008–1011.
16. Myrow, P. M. *et al.*, Integrated tectonostratigraphic analysis of the Himalaya and implications for its tectonic reconstruction. *Earth Planet. Sci. Lett*., 2003, **212**, 433–441.
17. Bernet, M., Van der Beek, P. A., Pik, R., Huyghe, P., Mugnier, J. L., Labrin, E. and Szulc, A., Miocene to Recent exhumation of the central Himalaya determined from combined detrital zircon fission-track and U/Pb analysis of Siwalik sediments, western Nepal. *Basin Res.* (in press).

18. Parkash, B., Sharma, R. P. and Roy, A. K., The Siwalik Group (molasse) sediments shed by collision of continental plates. *Sediment. Geol.*, 1980, **25**, 127–159.
19. Tandon, S. K., The Himalayan Foreland: focus on Siwalik Basin. In *Sedimentary Basins of India: Tectonic Context* (eds Tandon, S. K., Pant, C. C. and Casshyap, S. M.), Gyanodaya Prakashan, Nainital, 1991, pp. 177–201.
20. Burbank, D. W., Beck, R. A. and Mulder, T., The Himalayan foreland basin. In *The Tectonic Evolution of Asia* (eds Yin, A. and Harrison, M.), Cambridge University Press, New York, 1996, pp. 149–188.
21. Brozovic, N. and Burbank, D. W., Dynamic fluvial systems and gravel progradation in the Himalayan foreland. *Geol. Soc. Am. Bull.*, 2000, **112**, 394–412.
22. Kumar, R., Ghosh, S. K. and Sangode, S. J., Mio–Pliocene sedimentation history in the northwestern part of the Himalayan foreland basin, India. *Curr. Sci.*, 2003, **84**, 1006–1013.
23. Kumar, R., Ghosh, S. K. and Sangode, S. J., Depositional environment of Mio–Pliestocene coarse clastic facies in the Himalayan Foreland Basin, India. *Himalayan Geol.*, 2004, **25**, 101–120.
24. Critelli, S. and Ingersoll, R. V., Sandstone petrology and provenance of the Siwalik Group (northwestern Pakistan and western-southeastern Nepal). *J. Sediment. Res.*, 1994, **A64**, 815–823.
25. Ghosh, S. K. and Kumar, R., Petrography of Neogene Siwalik sandstone of the Himalayan foreland basin, Garhwal Himalaya: implications for source-area tectonics and climate. *J. Geol. Soc. India*, 2000, **55**, 1–15.
26. Sangode, S. J. and Kumar, R., Magnetostratigraphic correlation of the Late Cenozoic fluvial sequences from NW Himalaya, India. *Curr. Sci.*, 2003, **84**, 1014–1024.
27. Opdyke, N. D., Lindsay, E. H., Johnson, G. D., Tahirkheli, R. A. K. and Mirza, M. A., Magnetic polarity stratigraphy and vertebrate paleontology of the Upper Siwalik Subgroup of northern Pakistan. *Palaeogeogr., Palaeoclimatol., Palaeoecol.*, 1979, **27**, 1–34.
28. Johnson, N. M., Sticks, J., Tauxe, L., Cerveny, P. F. and Tahirkheli, R. A. K., Palaeomagnetic chronology fluvial process and implications of the Siwalik deposits near Chinji Village, Pakistan. *J. Geol.*, 1985, **93**, 27–40.
29. Sangode, S. J., Kumar, R. and Ghosh, S. K., Magnetic polarity stratigraphy of the Siwalik sequence of Haripur area (H.P.), NW Himalaya. *J. Geol. Soc. India*, 1996, **47**, 683–704.
30. Sangode, S. J., Kumar, R. and Ghosh, S. K., Magnetic polarity stratigraphy of the Late Miocene Siwalik Group sediments from Kangra Re-entrant, H.P., India. *Himalayan Geol.*, 2003, **24**, 47–61.
31. Sangode, S. J., Kumar, R. and Ghosh, S. K., Palaeomagnetic and rock magnetic perspectives on the post collision continental sediments of the Himalaya. In *The Indian Subcontinent and Gondwana: A Palaeomagnetic and Rock Magnetic Perspective* (eds Radhakrishna, T. and Piper, J. D. A.), Mem. Geol. Soc., India, 1999, vol. 44, pp. 221–248.
32. Rathi, G., Sangode, S. J., Kumar, R. and Ghosh, S. K., Magnetic fabrics under high-energy fluvial regime of the Himalayan Foreland Basin, NW Himalaya. *Curr. Sci.*, 2006, **92**, 933–944.
33. Sinha, S., Sangode, S. J., Kumar, R. and Ghosh S. K., Accumulation history and tectonic significance of the Neogene continental deposits in the west central sector of the Himalayan foreland basin. *Himalayan Geol.*, 2005, **26**, 387–408.
34. Raiverman, V., Foreland sedimentation. In *Himalayan Tectonic Regime. A Relook at the Orogenic Process*, Bishen Singh Mahendra Pal Singh, 2002, p. 371.
35. Sinha, S., Kumar, R., Ghosh, S. K. and Sangode, S. J., Controls on expansion–contraction of late Cenozoic alluvial architecture: A case study from the Himalayan Foreland Basin, NW Himalaya, India. *Himalayan Geol.*, 2007, **28**, 1–22.
36. Jelinek, V., Characterization of the magnetic fabric of rocks. *Tectonophysics*, 1981, **79**, 63–67.
37. DeCelles, P. G., Gehrels, G. E., Quade, J., Ojha, T. P., Kapp, P. A. and Upreti, B. N., Neogene foreland basin deposits, erosional unroofing, and the kinematic history of the Himalayan fold-thrust belt, western Nepal. *Geol. Soc. Am. Bull.*, 1998, **110**, 2–21.
38. Tandon, S. K., Siwalik sedimentation in a part of the Kumaun Himalaya, India. *Sediment. Geol.*, 1976, **16**, 131–154.
39. White, N. M., Parrish, R. R., Bickle, M. J., Najman, Y. M. R., Burbank, D. and Maithani, A., Metamorphism and exhumation of the NW Himalaya constrained by U–Th–Pb analyses of detrital monazite grains from early foreland basin sediments. *Geol. Soc. London*, 2001, **158**, 625–635.
40. Appel, E., Rosler, W. and Corvinus, G., Magnetostratigraphy of the Miocene–Pleistocene Surai Khola Siwaliks in West Nepal. *Geophys. J. Int.*, 1991, **105**, 191–198.
41. Hrouda, F., Magnetic anisotropy of rocks and its application in geology and geophysics. *Geophys. Surv.*, 1982, **5**, 37–82.
42. Gilder, S., Chen, Y. and Sen, S., Oligo–Miocene magnetostratigraphy and rock magnetism of the Xishuigou section, Subei (Gansu Province, western China) and implications for shallow inclinations in Central Asia. *J. Geophys. Res.*, 2001, **106**, 505–521.
43. Singh, B. P. and Lee, Yong II, Atmospheric $pCO_2$ and climate during late Eocene (36 ± 5 Ma) on the Indian subcontinent. *Curr. Sci.*, 2007, **92**, 518–523.
44. Sun, J., Zhua, R. and An, Z., Tectonic uplift in the northern Tibetan Plateau since 13.7 Ma ago inferred from molasse deposits along the Altyn Tagh Fault. *Earth Planet. Sci. Lett.*, 2005, **235**, 641–653.
45. Dettman, D. L., Kohn, M. J., Quade, J., Ryerson, F. J., Ojha, T. P. and Hamidullah, S., Seasonal stable isotope evidence for a strong Asian monsoon throughout the past 10.7 m.y. *Geology*, 2001, **29/1**, 31–34.
46. Sanyal, P., Bhattacharya, S. K., Kumar, R., Ghosh, S. K. and Sangode, S. J., Mio–Pliocene monsoonal record from Himalayan Foreland basin (Indian Siwalik) and its relation to the vegetational change. *Palaeogeogr., Palaeoclimatol., Palaeoecol.*, 2004, **205**, 23–41.
47. Karunakaran, C. and Ranga Rao, A., Status of exploration for hydrocarbons in the Himalayan region – contributions to stratigraphy and structure. *Geol. Surv. India Misc. Pub.*, 1976, **41/V**, 1–66.
48. Sinha, S., Islam, R., Ghosh, S. K., Kumar, R. and Sangode, S. J., Geochemistry of Neogene Siwalik mudstones along Punjab re-entrant, India: implications for source area weathering, provenance and tectonic setting. *Curr. Sci.*, 2007, **92**, 1103–1113.


ACKNOWLEDGEMENTS. We thank Prof. B. R. Arora, Director, Wadia Institute of Himalayan Geology, Dehra Dun, and Principal, DBS College for providing the necessary facilities. This work is financially supported by a DST sponsored project and is a part of the Ph D thesis of S.S.

Received 27 August 2007; revised accepted 6 November 2008